Bulletin of Earthquake Engineering (2022) 20:7737–7762
https://doi.org/10.1007/s10518-021-01251-5

S.I.: THE M7.0 SAMOS ISLAND (AEGEAN SEA) EARTHQUAKE OF 30TH OCTOBER 2020

The Samos Island (Aegean Sea) M7.0 earthquake: analysis and engineering implications of strong motion data

Aysegul Askan[1] · Zeynep Gülerce[1] · Zafeiria Roumelioti[2] · Dimitris Sotiriadis[3] · Nikolaos S. Melis[4] · Abdullah Altindal[1] · Burak Akbaş[1] · Eyüp Sopaci[5] · Shaghayegh Karimzadeh[1,9] · Ioannis Kalogeras[4] · Nikolaos Theodoulidis[6] · Kiriaki Konstantinidou[6] · A. Arda Özacar[7] · Özkan Kale[8] · Basil Margaris[6]

Received: 1 May 2021 / Accepted: 11 October 2021 / Published online: 15 November 2021

Abstract
We present a dataset of 77 strong ground motion records within 200 km epicentral distance from the 30 October 2020, M7.0 Samos Island (Aegean Sea) earthquake, which affected Greece and Turkey. Accelerograms from National Networks of both countries have been merged into a single dataset, including metadata that have been uniformly derived using a common preliminary source model. Initial findings from the analysis and comparative examination of acceleration time histories, Fourier amplitude spectra and 5%-damped response spectra are discussed along with significant source, propagation path and site effects. The long-period amplifications observed in most records in Izmir bay triggered failures and severe damages in weak structures. Yet, the spectral accelerations are observed to lie below the current and previous design spectra corresponding to the damaged regions. Peak ground motions are used to construct a purely instrumental-based macroseismic intensity map, which is capable of reflecting the actual earthquake damage caused by this considerably large event. Finally, peak ground motions are compared to various ground motion models (GMMs) and deviations are highlighted. Our overall preliminary analysis reveals a strong energy signature of the Samos earthquake in the period range 0.5–1.5 s at many sites, both on rock and soil, whereas records in the heavily hit Izmir city, at an epicentral distance circa 70 km, provide strong indication for additional amplification due to basin effects. At relatively large distance from the earthquake source (> 120 km), several recorded amplitudes are significantly lower than those predicted by many GMMs, implying that further studies are necessary toward the improvement of regional attenuation models.

Keywords Samos earthquake 2020 · Strong motion · Macroseismic intensity · Ground motion models

✉ Aysegul Askan
aaskan@metu.edu.tr

Extended author information available on the last page of the article

1 Introduction

On October 30, 2020, an earthquake of magnitude M7.0 occurred to the north of Samos Island (eastern Aegean) with a normal focal mechanism, consistent with the zone of North–South extension in the region (Kiratzi et al. 2021). The earthquake was followed by a tsunami wave, which affected coastal areas close to the epicenter with more severe effects around the Sığacık Bay in Turkey and in northern Samos in Greece. Due to a combination of the strong ground motion and tsunami effects, 119 fatalities were observed. The vast majority were lost due to structural failures in İzmir city center (Western Turkey), with remarkably localized ground shaking effects in İzmir, despite the long distance from the source.

Immediately after the event, reconnaissance teams in the field noted the irregular pattern of damage distribution, which was largely concentrated in the city of Izmir, at a distance of circa 70 km from the epicenter, whereas regions much closer to the earthquake source appeared to be less affected. This fact implied complicated source, propagation path and/or site effects phenomena, which require a detailed study of ground motion data which is well-distributed across the heavily affected area. For this purpose, five Institutes and Associations from Greece, Turkey and the United States collected and merged data and reconnaissance observations from the two sides of the Aegean: The Hellenic Association of Earthquake Engineering (HAEE/ETAM), the Earthquake Engineering Association of Turkey (EEAT), the Earthquake Foundation of Turkey (EFT), the Earthquake Engineering Research Institute (EERI) and the Geotechnical Extreme Events Reconnaissance Association (GEER). The reconnaissance efforts in the form of technical reports are significant in assessing severe seismic events for a complete evaluation of all aspects involved (Ansal et al. 1999a, 1999b; Cetin et al. 2020; Cetin 2020; Margaris et al. 2008; Nikolaou et al., 2014).

In this work, we describe the results of the above-mentioned collaborative study associated with the strong ground motion records of the October 30, 2020 Samos earthquake. We initially present the joint dataset of accelerograms to study the distribution of various ground motion measures, such as peak amplitudes, durations and energy characteristics with regard to distance and site effects. We discuss the significant features of acceleration time histories as well as Fourier and response spectra of the selected records, followed by a discussion on potential correlations between the ground motion properties and observed damages. Next, spatial distribution of shaking intensity values, in terms of Modified Mercalli Intensity (MMI) in the meizoseismal area are studied. The spatial distribution of MMI values are maximum in Bayrakli region of severe damage and on Samos Island. Finally, we compare the ground motion data against a representative suit of Ground Motion Models (GMMs) including one very recently proposed for the Aegean region. The discussions and conclusions frame the major highlights of the recorded ground motions of the Samos earthquake with mention of potential future efforts related to the seismic hazard in the Greece-Turkey cross-border region.

2 Data

In this study, a dataset of 77 strong motion records was formed, from stations operated by different institutes/organizations in Turkey and Greece. More specifically, 66 records were obtained from the permanent monitoring stations of the Disaster and Emergency Management Presidency of Turkey (AFAD, https://en.afad.gov.tr/), 5 from stations of the Institute of Geodynamics of the National Observatory of Athens (NOA, http://accelnet.gein.noa.gr/) and 6 from stations of the Institute of Engineering Seismology and Earthquake Engineering (ITSAK, http://www.itsak.gr/en).

Basic processing such as de-trending, removal of glitches and other "non-standard" errors and filtering was applied separately to Greek and Turkish data to ensure that time series are free of any issues to ensure data quality. AFAD regularly publishes both unprocessed and processed data to the public, after the earthquakes. As part of its routine processing, AFAD applies the procedures described in Paolucci et al. (2011). Immediately after the 2020 Samos earthquake, AFAD officially released "automatic processed data", filtered with second-order Butterworth filter between cut-off frequencies of 0.1–25 Hz (https://tadas.afad.gov.tr), which we also adopt in this study. The strong motion data of the Greek stations were uniformly processed following the procedures described in Margaris et al. (2021) and Boore et al. (2021) and band pass filtered, based on signal-to-noise ratio criteria, which resulted in a low-cut frequency of 0.05 Hz for the majority of the Greek records.

The integrated dataset was supplemented by metadata on basic site parameters as well as distance metrics. The distance metrics are naturally dependent on the fault geometry adopted. Among several source models (e.g.: Akinci et al., 2021), in this study, the finite fault model proposed in Chapter 1 of Cetin et al. (2020) are used to compute various source-to-site-distance metrics of the recording stations. Akkar et al. (2021) underlines the effect of uncertainties in the rupture plane parameters on calculating the source-to-site distance metrics specifically for this earthquake. This uncertainty is also considered in Gülerce et al. (2021). However, since the near-fault records are limited in number for this event, the mentioned uncertainty is not deemed to be critical. Distance parameters provided, include the Joyner-Boore distance (R_{JB}), rupture distance

Table 1 Geometric description of the source model used to calculate distance metrics for the stations in the herein presented merged dataset

Parameter	Value	Explanation/reference
Rupture length, Rupture width	32 km 15 km	Cetin et al. (2020)
Rupture center	37.892° 26.807°	Imposing stronger propagation to the west, where the largest slip patch is reported (Cetin et al., 2020)
Strike / Dip	270°/ 45°	Cetin et al. (2020)
Z_{TOR}	0–2 km	Z_{TOR} = 0.6 km is used for distance metrics and 1 km resolution in computations is given in Cetin et al. (2020)
Max. rupture depth	11.2 km	Cetin et al. (2020)

Table 2 Information on strong ground motion records of Samos earthquake for 35 stations within 100 km epicentral distance [R_{JB}: closest distance to the horizontal surface projection of the rupture plane as defined in Joyner and Boore (1981); R_{RUP}: closest distance to the rupture plane; R_{EPI}: epicentral distance]. Site classification of Greek stations (SMG1 and SAMA) follows the scheme of Eurocode 8 (EC8, 2004), whereas that of Turkish stations the scheme of the 2019 edition of the building code in Turkey (TBEC, 2019)

Station Code	Name	Lat. (°)	Long. (°)	R_{JB} (km)	R_{RUP} (km)	R_{EPI} (km)	Vs30 (m/s)	Site Class	Comp	PGA (cm/s^2)	PGV (cm/s)	PGD (cm)	Significant Duration (s)	Arias Intensity (cm/s)	Housner Intensity (cm)
SMG1	Vathi	37.7561	26.9762	9.59	9.60	23.23	550	B	N42°	227.30	21.49	8.38	12.09	36.49	53.80
									N312°	157.80	19.88	5.96	12.26	55.82	57.92
									U-D	134.02	11.16	5.51	15.12	14.24	23.24
SAMA	Vathi	37.7537	26.9806	10.03	10.05	22.38	840	A	N225°N225	166.31	16.00	2.84	10.29	34.81	51.70
									N135°	120.32	17.37	3.78	11.38	23.05	48.79
									U-D	99.68	6.77	2.28	14.16	10.82	21.26
0905	Aydın Kuşadası Meteoroloji Müdürlüğü	37.8600	27.2650	31.52	31.69	42.95	369	C	E-W	144.02	8.93	2.26	16.61	20.37	35.60
									N-S	179.31	7.85	1.50	15.43	21.81	32.61
									U-D	79.84	4.56	1.35	17.88	8.38	20.13
0911	Aydın Söke Yenikent	37.7621	27.3909	42.90	42.91	55.71	307	D	E-W	66.66	4.54	1.84	25.56	7.51	21.34
									N-S	48.01	4.31	1.06	23.88	7.64	20.93
									U-D	47.47	2.78	1.61	25.55	4.55	10.09
0918	Aydın Didim Hükümet Konağı	37.3697	27.2643	59.43	59.43	71.86	630	C	E-W	30.99	4.98	2.15	29.21	4.56	21.65
									N-S	38.19	5.99	3.06	29.91	5.05	27.23
									U-D	20.96	4.09	1.19	37.79	2.62	21.58
0919	Aydın Karpuzlu Halk Eğitim Merkezi	37.5595	27.8355	86.67	86.67	100.01	986	B	E-W	17.95	1.03	0.75	30.74	0.54	4.09
									N-S	21.40	1.22	0.70	26.59	0.65	4.53
									U-D	14.86	1.21	0.92	32.28	0.33	4.80
0920	Aydın Sarıkemer Belediye	37.5604	27.3749	50.39	50.40	63.98	894	B	E-W	30.69	2.71	1.27	19.57	1.54	11.37
									N-S	25.68	3.00	1.95	21.70	1.45	12.45
									U-D	21.98	1.99	1.06	24.58	0.55	5.37

Table 2 (continued)

Station Code	Name	Lat. (°)	Long. (°)	R_{JB} (km)	R_{RUP} (km)	R_{EPI} (km)	Vs30 (m/s)	Site Class	Comp	PGA (cm/s^2)	PGV (cm/s)	PGD (cm)	Significant Duration (s)	Arias Intensity (cm/s)	Housner Intensity (cm)
0921	Aydın Germencik Devlet Hastanesi	37.8747	27.5922	60.15	60.33	71.56	None	None	E-W	70.85	8.47	3.23	30.85	13.14	37.22
									N-S	55.03	4.94	1.37	36.60	8.35	27.61
									U-D	23.06	3.11	1.06	38.76	3.07	16.04
0922	Aydın İncirliova Spor Lisesi	37.8537	27.7082	70.26	70.32	81.83	None	None	E-W	58.60	5.17	2.62	40.15	11.20	24.81
									N-S	60.05	4.93	3.11	46.91	9.68	22.94
									U-D	56.46	1.84	0.86	32.09	5.00	9.60
3506	İzmir Konak Güzelyalı Meteoroloji Müdürlüğü	38.3944	27.0821	54.99	56.12	62.30	771	B	E-W	41.04	3.17	0.92	20.33	3.43	16.17
									N-S	43.88	3.39	0.91	20.44	3.89	12.91
									U-D	23.59	2.07	0.91	26.69	1.66	9.55
3511	İzmir Pınarbaşı Bornova	38.4213	27.2563	63.57	64.55	72.61	827	B	E-W	41.29	5.98	1.51	22.11	2.03	23.03
									N-S	29.11	3.96	1.08	21.36	2.48	17.60
									U-D	18.90	1.87	0.65	30.41	0.82	10.09
3512	İzmir Buca Gürçeşme Zübeyde Hn Huzurevi	38.4009	27.1516	57.63	58.71	65.76	468	C	E-W	56.75	3.90	1.14	25.59	8.21	18.16
									N-S	57.54	3.31	1.16	24.99	7.93	17.01
									U-D	28.16	1.58	0.78	26.28	2.60	8.36
3513	İzmir Bayraklı ÇŞB İl Müd	38.4584	27.1671	64.08	65.05	72.00	196	D	E-W	94.67	14.42	3.15	20.16	35.30	84.81
									N-S	106.28	17.11	2.90	20.59	33.17	79.76
									U-D	44.19	4.48	0.80	30.84	6.42	23.29
3514	İzmir Bayraklı Sağlık Evi	38.4762	27.1581	65.67	66.62	73.39	836	B	E-W	56.02	6.41	1.31	23.75	4.58	28.26
									N-S	39.42	4.23	1.44	25.90	3.52	22.39
									U-D	25.15	1.94	0.73	27.17	2.10	10.91

Table 2 (continued)

Station Code	Name	Lat. (°)	Long. (°)	R_{JB} (km)	R_{RUP} (km)	R_{EPI} (km)	Vs30 (m/s)	Site Class	Comp	PGA (cm/s^2)	PGV (cm/s)	PGD (cm)	Significant Duration (s)	Arias Intensity (cm/s)	Housner Intensity (cm)
3516	İzmir Güzelbahçe Belediye Spor Salonu	38.3706	26.8907	50.22	55.75	54.57	460	C	E-W	48.36	3.63	1.30	20.67	5.35	17.35
									N-S	47.29	4.84	1.19	21.65	4.85	20.13
									U-D	32.08	2.44	1.05	24.15	2.49	9.72
3517	İzmir Buca DEU	38.3756	27.1936	56.54	57.64	65.32	695	C	E-W	36.14	3.50	1.28	25.69	2.73	16.94
									N-S	40.10	3.95	1.11	24.67	2.86	16.15
									U-D	19.82	2.11	0.79	34.71	1.69	11.45
3518	İzmir Konak Fuar Kulturpark Tenis Kulubu	38.4312	27.1435	60.53	61.56	68.36	298	D	E-W	91.45	10.65	2.70	18.81	31.94	67.85
									N-S	106.10	11.33	1.61	25.03	23.66	56.05
									U-D	31.14	8.33	5.16	19.06	4.52	23.47
3519	İzmir Karşıyaka Orman İl Müdürlüğü	38.4525	27.1112	61.90	62.91	69.23	131	E	E-W	109.98	14.48	3.24	23.17	35.95	76.79
									N-S	150.09	22.53	3.93	20.58	45.60	92.24
									U-D	34.17	4.33	1.05	31.06	6.00	22.86
3520	İzmir Manavkuyu Halk Kütüphanesi	38.4780	27.2111	67.53	68.46	75.78	875	B	E-W	58.55	8.37	2.04	19.73	5.21	36.08
									N-S	36.11	4.65	1.13	20.11	3.60	24.21
									U-D	19.37	2.68	0.70	26.80	1.33	13.63
3521	İzmir Mavişehir Karşıyaka Bel	38.4679	27.0764	62.76	63.76	69.58	145	E	E-W	93.99	12.29	3.14	26.06	29.47	66.66
									N-S	110.84	16.17	4.08	22.61	35.19	87.41
									U-D	40.31	3.86	1.14	30.03	6.49	23.70
3522	İzmir Çamdibi Sağlık Ocağı	38.4357	27.1987	62.79	63.78	71.18	249	D	E-W	63.94	14.81	2.77	24.49	13.37	55.71
									N-S	73.72	9.92	2.56	20.55	19.25	49.83
									U-D	24.65	3.72	0.71	30.13	2.32	18.42

Table 2 (continued)

Station Code	Name	Lat. (°)	Long. (°)	R_{JB} (km)	R_{RUP} (km)	R_{EPI} (km)	Vs30 (m/s)	Site Class	Comp	PGA (cm/s^2)	PGV (cm/s)	PGD (cm)	Significant Duration (s)	Arias Intensity (cm/s)	Housner Intensity (cm)
3523	İzmir Urla Kapalı Spor Salonu	38.3282	26.7706	45.50	51.14	48.94	414	C	E-W	63.57	4.99	1.43	22.08	10.38	22.26
									N-S	80.32	5.73	1.93	20.46	10.91	30.20
									U-D	36.90	4.11	1.97	26.85	4.30	17.62
3524	İzmir Yamanlar Müyesser Turfan Güçsüzler Evi	38.4969	27.1073	66.55	67.49	73.59	459	C	E-W	68.34	5.90	0.98	16.98	9.24	24.91
									N-S	64.71	4.74	0.94	18.91	7.29	19.38
									U-D	29.83	1.93	0.62	24.94	2.55	7.71
3526	İzmir-Menemen-Seyrek	38.5782	26.9795	73.56	74.41	78.75	205	D	E-W	81.50	10.45	2.27	31.43	20.33	53.04
									N-S	88.77	10.82	3.19	24.44	25.36	61.01
									U-D	29.15	3.41	0.86	38.81	3.83	18.82
3527	İzmir-Karaburun-Halk Eğitim	38.6390	26.5128	80.11	80.89	86.63	207	D	E-W	56.57	7.03	1.76	13.75	6.68	38.13
									N-S	80.93	8.85	2.62	15.07	10.66	47.62
									U-D	46.65	6.07	1.03	17.25	4.15	22.87
3528	İzmir Çeşme Ilıca Meteoroloji Müdürlüğü	38.3039	26.3726	45.38	46.75	58.23	532	C	E-W	149.31	8.36	1.89	12.90	31.26	40.95
									N-S	117.57	7.57	2.26	14.77	14.33	32.67
									U-D	77.00	3.63	1.49	16.82	6.75	14.52
3533	İzmir Menderes Sağlık Grup Başkanlığı	38.2572	27.1302	42.29	43.75	51.38	415	C	E-W	45.90	5.95	1.89	25.16	7.53	26.11
									N-S	73.64	5.52	2.31	27.21	8.49	27.29
									U-D	37.46	3.39	1.14	29.36	3.81	18.20
3534	İzmir-Foça-Reha	38.6624	26.7586	82.66	87.77	86.11	328	D	E-W	92.48	4.91	0.94	19.00	14.52	20.58
									N-S	73.16	5.09	0.68	17.00	16.09	23.37
									U-D	38.31	2.63	0.69	24.42	2.39	10.09

Table 2 (continued)

Station Code	Name	Lat. (°)	Long. (°)	R_{JB} (km)	R_{RUP} (km)	R_{EPI} (km)	Vs30 (m/s)	Site Class	Comp	PGA (cm/s^2)	PGV (cm/s)	PGD (cm)	Significant Duration (s)	Arias Intensity (cm/s)	Housner Intensity (cm)
3536	İzmir Seferihisar Hükümet Konağı	38.1968	26.8384	30.89	37.02	34.75	1141	B	E-W	79.14	8.71	2.13	17.48	8.06	27.31
									N-S	50.22	5.32	1.88	19.42	5.12	21.51
									U-D	31.32	3.57	1.12	22.07	2.56	11.37
3538	İzmir Gaziemir Toplum Sağlık Merkezi	38.3187	27.1233	48.24	49.52	56.67	None	None	E-W	76.95	6.08	1.24	22.00	15.44	29.66
									N-S	85.48	5.48	1.11	23.88	12.36	27.32
									U-D	39.26	2.66	0.83	25.76	5.18	15.53
3539	İzmir Tire Devlet Hastanesi	38.1023	27.7211	74.01	74.85	86.09	None	None	E-W	27.02	1.94	0.52	28.38	1.67	9.57
									N-S	37.63	2.68	1.43	27.03	2.44	11.40
									U-D	22.25	1.75	0.93	30.93	1.05	8.84
4501	Manisa-Merkez-ÇŞB Müd	38.6126	27.3814	87.46	88.17	96.31	340	D	E-W	40.00	6.81	1.78	23.61	4.68	29.15
									N-S	34.89	7.06	1.41	21.83	4.31	30.71
									U-D	24.36	3.54	1.16	36.12	2.25	20.10
4814	Muğla Selimiye Orman İşletme	37.3991	27.6567	81.05	81.06	94.63	694	C	E-W	23.23	1.09	0.64	22.72	0.35	4.35
									N-S	25.33	1.63	1.09	20.54	0.58	7.05
									U-D	10.22	1.30	0.64	26.01	0.21	4.11
4822	Muğla Milas Derince Barajı- Crest	37.4417	27.6460	77.58	77.58	91.18	None	None	E-W	80.06	5.39	0.97	19.05	12.46	20.70
									N-S	32.52	1.68	0.82	38.61	2.87	6.79
									U-D	37.98	2.04	0.76	27.76	2.46	7.77
4823	Muğla Milas Derince Barajı- Bedrock	37.4418	27.6440	77.43	77.43	91.03	None	None	E-W	25.77	1.60	0.86	22.95	1.17	8.17
									N-S	22.77	1.38	0.79	25.57	0.86	4.76
									U-D	18.57	1.66	0.74	26.15	0.58	5.63

(R_{RUP}), and other site-specific distance measures that depend on the source-to-site azimuth (R_x and R_{y0}). The finite fault parameters used in calculating the distance metrics (and the parameters used in estimating the prediction performance of GMMs) are summarized in Table 1. Table 2 lists location information for the 35 stations closest to the source, as well as, three different distance metrics: R_{JB} as defined in Joyner and Boore (1981), R_{RUP} and the epicentral distance, R_{EPI}. Figure 1 presents the distribution of stations in our dataset around the source area. Square symbols mark the locations of stations at distance less than 100 km from the epicenter, which are analyzed in more detail in the next section, whereas the remaining station locations, up to 200 km distance, are shown with triangles. The entire dataset has been used in comparisons with empirical GMMs, as described in Sect. 5.

Table 2 also includes peak ground motion values (Peak Ground Acceleration, PGA; Peak Ground Velocity, PGV; Peak Ground Displacement, PGD), Arias and Housner intensities, and significant duration (calculated as the time between 5 and 95% of the cumulative Arias Intensity) for all stations and components. We note that PGD values are highly sensitive to the high-pass filter cut off values. Corresponding information for stations beyond 100 km from the earthquake source is provided in the Online Resource 1.

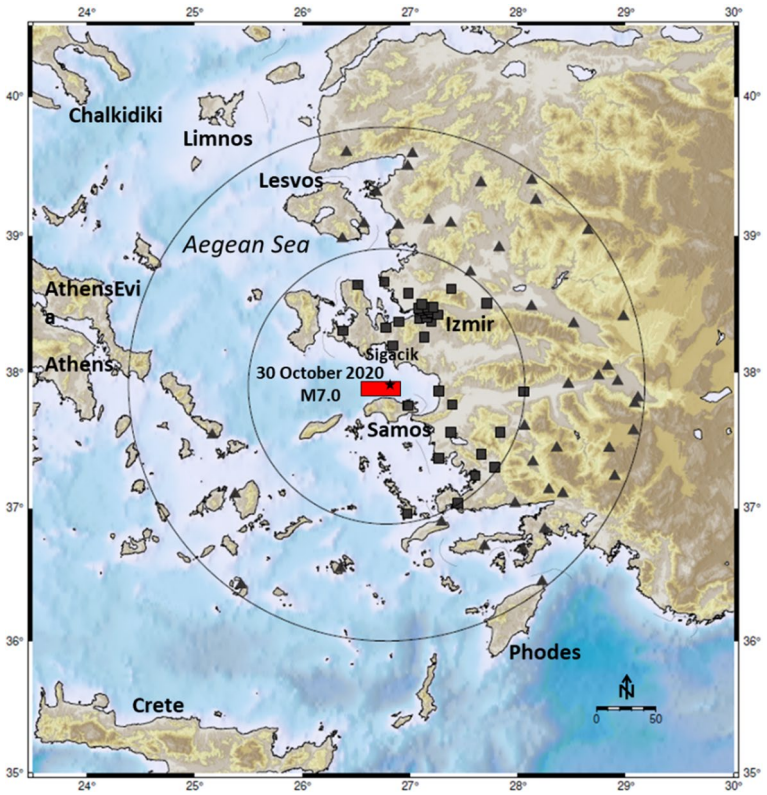

Fig. 1 Spatial distribution of the merged set of strong motion stations around the source of the M7.0 Samos earthquake. Surface projection of the adopted north-dipping fault plane (Cetin et al. 2020) is shown as red rectangle. Earthquake epicenter is marked by the black star symbol. Stations at distance < 100 km are shown as squares (inner circle), whereas the remaining, up to 200 km are shown as triangles (outer circle)

Additional information in the distributed metadata includes the values of average shear-wave velocity over the top 30 m of the soil columns, V_{S30}, at the recording sites. These values were used as proxies to consider site effects and assign geotechnical classes to recording sites. Geotechnical classification was performed according to Eurocode 8 and the current seismic code of Turkey (Turkey Building Earthquake Code—TBEC, 2019). The distribution of stations in terms of V_{s30} values and distance metrics are presented in Fig. 2. Most V_{S30} values are based on measured shear-wave velocity profiles provided by the national monitoring networks, whereas a small number has been extracted from the USGS V_{S30} worldwide map and/or incorporating additional factors related to surface geology and topographic slope (i.e., Allen and Wald 2009; Stewart et al. 2014). Shear-wave velocity values at the two strong motion stations on Samos Island (SMG1 and SAMA) were measured after the 30 October 2020 earthquake (Pelekis P., personal communication). The V_{S30} values assigned to the 77 station sites discussed in this work and corresponding geotechnical classifications are included in the **Online Resource 1**.

3 Analysis of ground motion records

The 77 strong ground motion records within 200 km epicentral distance from the Samos M7.0 main shock, which are processed and presented in this study, exhibit considerable variability in terms of azimuth, source-to-site distance and site classes. Figure 3 shows the locations of eight selected stations to be discussed in more detail. These stations are particularly selected since they are located either at close distances from the epicenter with highest ground motion values and/or near the areas with severe structural damages. Acceleration time histories, Fourier Amplitude Spectra (FAS) and the 5%-damped response spectra from these stations are shown in Fig. 4. The 5%-damped acceleration response spectra are compared against the design spectra of the current and previous seismic codes of Turkey (CSCDA, 1975; CBCEA, 2007; TBEC, 2019) and Greece (EAK, 2000; EC8). Corresponding plots for all records up to 100 km distance from the earthquake source are provided in the **Online Resource 2**.

The two closest stations to the causative fault, SMG1 and SAMA, are located on Samos Island. Both stations are located on the footwall according to the preferred rupture plane model. The highest observed values of PGA = 0.23 g and PGV = 24 cm/s are both recorded

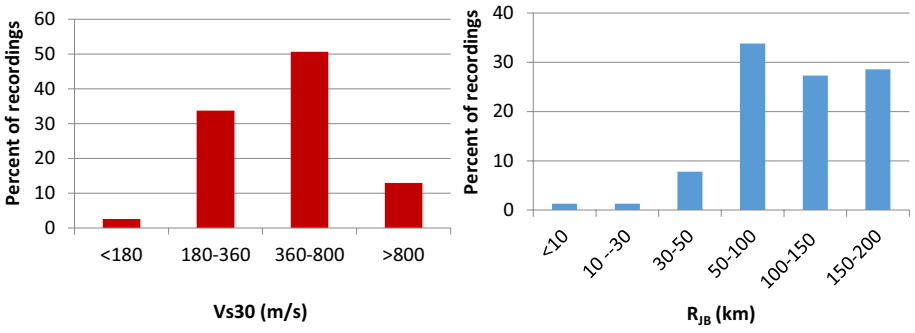

Fig. 2 Percentages of recording stations in each site class defined in TBEC19 and EC8 left) and percentages of recording stations in each distance bin (right)

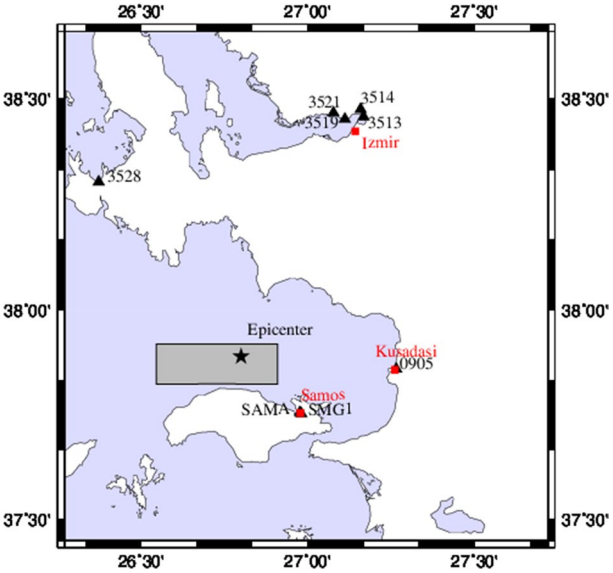

Fig. 3 Close-up view of the selected strong motion stations whose records are discussed in detail in the text

at SMG1. The surface geology at this station consists of Quaternary alluvial deposits with a measured V_{S30}≈550 m/sec. The accelerograph is installed at the basement of a typical 3-story reinforced concrete (R/C) building. Nearby, at SAMA station, surface geology is composed of metamorphic Paleozoic formations (marble) with a measured V_{S30}≈840 m/sec. The station SAMA is also installed at the basement of a 3-story R/C building.

Station 0905 (Figs. 3, 4) is located at the shortest epicentral distance among the stations in Turkey. It is installed on stiff soil (V_{S30} = 369 m/s) in the town of Kusadasi (Aydin province) and recorded a PGA value of 0.18 g. FAS and response spectra for this record indicate short-period amplification within 0.2–0.33 s range (3–5 Hz range in frequency domain), yet no significant structural damage was observed near this site. Station 3528 (Figs. 3, 4), located in town Çeşme Ilıca, is deployed also on stiff soil (V_{S30} = 532 m/s), recorded a PGA value of 0.15 g and shows short-period amplification as well. Two stations 3519 and 3521 (Figs. 3, 4) are located in Karşıyaka district, İzmir, on soft soil (V_{S30} = 131 m/s and 145 m/s, respectively). The records at these two stations display long-period amplification up to 1 s and 1.5 s, respectively. Stations 3513 and 3514 (Figs. 3, 4) are both located in Bayraklı district, close to the most structural failures, on soft soil (V_{S30} = 196 m/s, site class D) and rock (V_{S30} = 836 m/s, site class B), respectively. At station 3513, despite the low recorded PGA level of 0.1 g, a clear long-period amplification can be noted up to 1.5 s. At 3514, on rock conditions in the same district, no similar amplification is observed. However, the elevated energy of Samos earthquake within a well-defined range of significantly long periods (0.5–1.5 s) is present in other rock station records from the Izmir Bay area (i.e. 3506, 3411, 3514, 3517 and 3520, time histories and spectra shown in the Online Resource 2).These already intense rock shaking levels in the period range of 0.5 to 1.5 s, have been further amplified inside the deep alluvial formations of Izmir Basin (especially at Konak and Bayraklı districts) with similar natural periods, leading to resonance phenomena. The long-period content noted at Station 3513 in Bayraklı (Figs. 3, 4), could help to explain the immense structural damage in several 7–9 story structures, as a combination

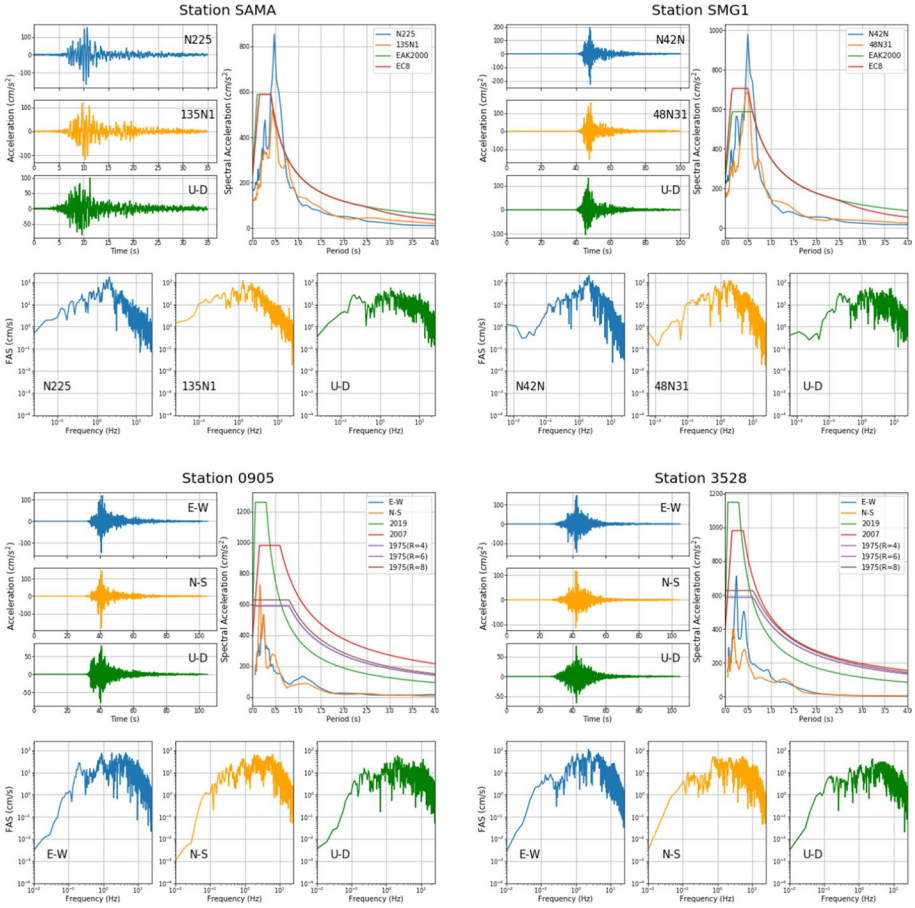

Fig. 4 Examples of acceleration time histories, Fourier amplitude spectra and 5%-damped response spectra of three-component recordings at 8 stations around the 2020 Samos earthquake source. In pertinent subplots, acceleration response spectra of records at Greek stations are compared to the design spectra of building codes currently in use in Greece (EAK, 2000 and EC8) and response spectra of records at Turkish stations are compared to design spectra of current and previous versions of the Turkish building code (TBEC, 2019)

of basin effects and poor structural design. The long significant durations and higher Housner intensities of records in this region also support this explanation (Table 2). Considering the entire set of records, elevated long-period content and overall longer significant durations are observed at softer sites, particularly at those located within the İzmir Bay, implying the emergence of significant basin effects. Consistently, the maximum PGV values recorded in Turkey for this event are observed at stations 3519 and 3513, with values around 23 and 17 cm/s, respectively. To assess the spectral effects and long-period content more closely, velocity response spectra at these stations are also presented in Fig. 5. It is observed that horizontal response spectral velocities at stations 3513 reach high values of 70 cm/s near periods of 1.3 s. At station 3519, the peak values occur around 1 s period with amplitudes of 57 m/s and 75 m/s in NS and EW directions, respectively. At the rock station 3514, the spectral velocities do not exceed

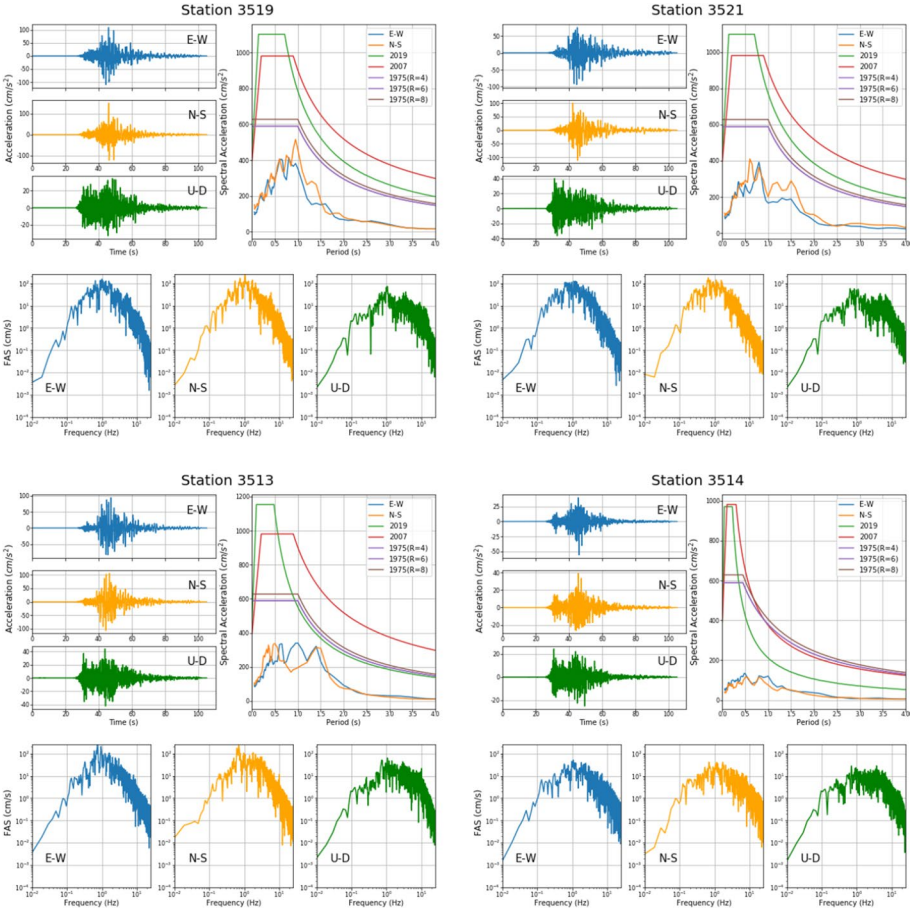

Fig. 4 (continued)

20 m/s for the horizontal components. All of these observations are consistent with the damages and failures observed in 7–10 story structures having periods around 0.9–1.3 s in the area.

With respect to building codes, it is observed that the acceleration response spectra at all stations in Turkey lie below the design spectra defined in the current earthquake code for Turkey (Turkey Building Earthquake Code—TBEC, 2019). The corresponding comparisons in Fig. 4 indicate that the same conclusion holds for the design spectra defined in the previous seismic codes in Turkey published in 2007 and 1975. These versions are assessed herein, as most buildings in regions with significant damages were built when these two previous codes were in effect. On the other hand, at stations 0905 and 3528 (Fig. 4), within a narrow band below 0.25 s, the response spectra slightly surpass the equivalent elastic spectra obtained from the inelastic design spectra (load reduction factors of R = 4, 6 and 8) of the 1975 edition of the Turkish earthquake code. However, no structural collapses have been reported in the vicinity of these stations. A similar comparison is observed for the stations in Greece: The elastic design spectra of seismic codes currently in use in Greece (EAK2000, Eurocode 8 – EC8) lie above the response

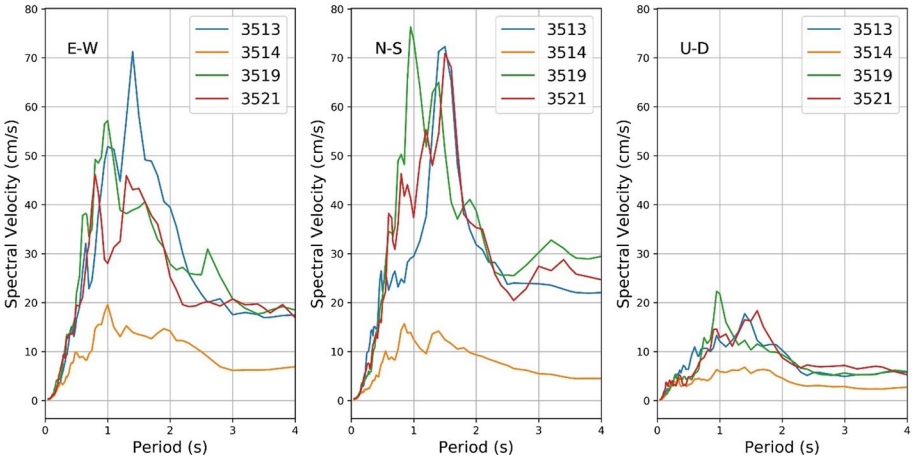

Fig. 5 Velocity response spectra of records at 4 selected ground motion stations (station codes are shown in the legends) in Izmir basin

spectra observed at the two stations on Samos Island for most periods except a narrow period band between 0.5 and 0.7 s.

4 Macroseismic intensities from recorded strong motions

To augment the instrumental intensity measures of ground motions, macroseismic intensity maps are used frequently to rapidly visualize spatial variation of ground shaking levels. These maps are valuable assessment tools despite the subjectivity involved in the assignment of intensity values. One way to assign intensities is to evaluate human response to ground shaking and damage observations, while an alternative is to obtain macroseismic intensity values from recorded motions. In the latter case, the subjectivity problem can also be overcome if a dense monitoring network operates in the earthquake affected area. In such cases, intensity values may be computed directly from observations, such as various peak ground motion measures. For this purpose, correlations between instrumental and felt intensity pairs are employed. Similarly, herein an intensity map in terms of Modified Mercalli Intensity (MMI) is prepared using the empirical equations of Bilal and Askan (2014). To obtain the MMI values, the actual peak ground motion values recorded at the 35 stations within 100 km epicentral distance have been used.

For the stations located on Samos Island, MMI-PGA correlations were used. This approach is consistent with the fact that the building stock on the island comprises basically typical low-rise buildings, mostly prone to damage from high-frequency shaking, which is better correlated with PGA. In Turkey, however, MMI-PGV correlations were used since PGV is well known to be a better indicator of damage in reinforced concrete structures (Erberik, 2008). The following relationships are employed to compute MMI values from observed PGA (in cm/s^2) and PGV (in cm/s), in Greece and Turkey respectively (Bilal and Askan 2014):

$$MMI = 0.132 + 3.884 \log (PGA) \tag{1}$$

$$MMI = 2.673 + 4.340 \log (PGV) \quad (2)$$

Figure 6 shows that the computed instrumental MMI on Samos Island is in the order of VII to VIII, in agreement with citizens reports and intensities published by the European-Mediterranean Seismological Center (EMSC, https://www.emsc-csem.org/). In addition, damage observed in various parts of the island (i.e., in Vathy and Karlovassi towns) by the reconnaissance teams of engineers indicate MMI values near VIII (e.g., Cetin et al. 2020). The coastal Gümüldür-Tepecik-Seferihisar-Sığacık region, which also suffered from the earthquake induced tsunami, exhibits MMI values of VI to VII. The Bayraklı district of İzmir, where severe structural damage took place, is attributed an estimated MMI value of VII to VIII. In general, Fig. 6 shows that the recorded PGA and PGV values, with their corresponding calculated MMI values, satisfactorily highlight regions of strongest shaking and damage, respectively.

5 Comparisons with ground motion models

The predictive performance of global GMMs (for shallow crustal earthquakes in active tectonic regions) in estimating the recorded strong ground motions from earthquakes in the broader area of the Samos earthquake (Turkey and Greece) has been evaluated by Gülerce et al. (2016), Akkar et al. (2018), Kale (2019), and Boore et al. (2021) in the last five years, using different analysis and ranking methods. Overall, previous efforts suggested that the global Next Generation Attenuation West 2 (NGA-W2) models developed by Abrahamson et al. (2014; ASK14), Boore et al. (2014; BSSA14), Campbell and Bozorgnia (2014; CB14) and Chiou and Youngs (2014; CY14), the most recent local GMM developed for Turkey by Kale et al. (2015; KAAH15) and the global NGA West 1 (NGA-W1) models adjusted for Turkey by Gülerce et al. (2016) performed well on several subsets of Turkish ground motion dataset.

Within the framework of this study, a collection of widely used GMMs has been chosen for comparison with the attenuation characteristics of the strong motion data

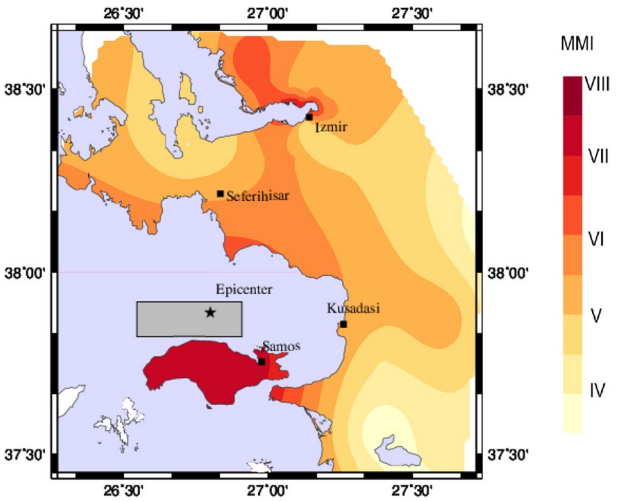

Fig. 6 Modified Mercalli Intensity (MMI) map for the 30 October 2020, M7.0 Samos earthquake based exclusively on recorded peak ground motion values

recorded within $R_{RUP} < 200$ km during the 2020 Samos earthquake. More specifically, we selected to compare the recorded data with the global NGA-W2 GMMs that are known to perform well in the broader study area (i.e., with high ranking scores from Kale, 2019); the model proposed by BSSA14, with three options for large distance scaling (the global model, the high-Q option proposed for China and Turkey and the low-Q option for Japan and Italy, where Q is the quality factor expressing anelastic attenuation) and the CY14 model. Additionally, the regional or regionalized GMMs for Turkey; the KAAH15 model and the Turkey-adjusted versions of the Abrahamson and Silva (2008; AS08) and the Chiou and Youngs (2008; CY08) GMMs are included in the comparisons. The TR-adjusted AS08 and CY08 models were chosen because they involve large-distance adjustments for $R_{RUP} = 100–200$ km to capture the region-specific distance attenuation of Turkish ground motion data. Detailed analysis of other global and TR-adjusted GMMs for predicting the Samos earthquake recordings collected by AFAD is provided in Gülerce et al. (2021).

To represent the regional GMMs developed for Greece, we chose to test a recently published model that has been developed based on accelerometric data from shallow (focal depth ≤ 30 km) crustal earthquakes in Greece (Boore et al. 2021). For this new GMM, a database of uniformly processed strong motion records has been utilized (Margaris et al. 2021) for predicting horizontal-component PGV, PGA, and 5%-damped pseudo-acceleration response spectra at 105 periods ranging from 0.01 to 10 s. The equations comprising the GMM were developed by modifying the model proposed by Boore et al. (2014) for low-Q regions (Italy, Japan), to account for more rapid attenuation and weaker magnitude scaling present in Greek ground motion data, which was not captured by global GMMs. This predictive model has been calibrated against the earthquake data in Greece of magnitude 4.0–7.0, recording site V_{S30} from 150 to 1200 m/s and distances up to 300 km. Specific features included in the model, allow its extension to larger magnitudes, up to M_w 8.0, as well as to nonlinear site response cases. The studies during the development of the new GMM revealed another interesting characteristic of Greek strong motion data, which was also observed in the Italian data: ground motion in Greece and Italy is substantially over-predicted by global GMMs. According to Boore et al. (2021), this may be attributed to specific regional features or may be a consequence of soil-structure interaction effects at the recording stations (very often installed inside medium-rise R/C public buildings). Therefore, a bias parameter, B, has been introduced in the model, which can be considered or not, in predictions of ground motion.

A detailed evaluation of the predictive performance of GMMs for this event is performed in Gülerce et al. (2021). In this study, GMMs are visually compared to the observed ground motions to investigate the general ground motion behaviors. To compare the distance attenuation characteristics of the 2020 Samos earthquake with the distance scaling of aforementioned GMMs, we used the entire set of records from all stations depicted in Fig. 1 ($R_{RUP} < 200$ km). In addition to PGA and PGV values listed in Table 2 (and included in the Online Resource 1), full waveforms were used in the computation of 5%-damped pseudo-spectral acceleration (PSA) at 111 spectral periods between 0.01 and 20 s. Based on the two horizontal components and for the 111 spectral periods, RotD50 (Boore 2010) values were calculated to facilitate comparisons with published GMMs. All these values are also provided as part of **Online Resource 1**. Two additional parameters required for the comparison for certain GMMs is the basin effect term, related to the depth of 1.0 and 2.5 km/s shear wave velocity horizons in the soil profile (denoted by $Z_{1.0}$ and $Z_{2.5}$). To compute this term, Eqs. 3 (Abrahamson and Silva 2008) and 4 (Campbell and Bozorgnia 2008) which were developed from the NGA-W1 database (Power et al., 2008) are utilized:

$$\ln\left(Z_{1.0}\right) = \begin{cases} 6.745 & for\ V_{s30} < 180\ \text{m/s} \\ 6.745 - 1.35 * \ln\left(\frac{V_{s30}}{180}\right) & for\ 180 \le V_{s30} \le 500\ \text{m/s} \\ 5.394 - 4.48 * \ln\left(\frac{V_{s30}}{500}\right) & for\ V_{s30} > 500\ \text{m/s} \end{cases} (inm) \quad (3)$$

$$Z_{2.5} = 0.519 + 3.595 * Z_{1.0}. \quad (4)$$

We evaluated the distance attenuation of recorded data against the distance scaling of selected GMMs in terms of RotD50 of the recordings at PGA and PSA at T = 0.2 s and T = 1 s, using R_{RUP} or R_{JB} (depending on the GMM) as distance metric. Pertinent comparisons are provided in Figs. 7, 8,9, 10, 11 and 12 for V_{S30} = 270 m/s (central V_{S30} value of site class D in TBEC-2019 and site class C in EN1998-1) and V_{S30} = 800 m/s (proxy of B/C boundary of TBEC-2019 and A/B boundary of EN1998-1). The median estimates of BSSA14 (global, high-Q option proposed for China and Turkey, and the low-Q option for Japan and Italy) and CY14 are presented in Figs. 7, 9 and 11 for different spectral periods. Similarly, the median predictions of the regional models (Boore et al. 2021, KAAH15, TR-adjusted AS08 and TR-adjusted CY08) are shown in Figs. 8, 10 and 12.

Figures 7, 9 and 11 show that the distance scaling of global GMMs is consistent with the recorded data, up to distances of 120 km. For longer distances, the BSSA14 model estimates for low-Q regions (Japan and Italy) follow the recorded data quite closely, whereas other models (BSSA14 with average or high-Q options and CY14) exhibit slower attenuation, which results in deviations from recorded ground motions. These observations are in accordance with the findings of previous studies for moderate-to-large magnitude events in Turkey (e.g. Akkar et al. 2011). Among the tested regional or regionally adjusted GMMs, the most recent model developed for Greece (Boore et al. 2021) with the modification of BSSA14 GMM for low-Q regions up to distances of 300 km, is consistent with recorded data for the entire distance range considered. Moreover, for this specific model, consideration of the bias factor B improves the fit of the model to the recorded data, especially at the two near-fault stations and at short periods (Figs. 8a and 10a). For three regional or regionally-adjusted models for Turkey, certain far-field stations present systematically lower ground motions than those expected, according to the median estimates of the models at PGA and PSA for T = 0.2 s. This overestimation, in accordance with the one observed with global GMMs, implies faster attenuation of higher frequencies beyond ~ 120 km distance.

At long spectral periods (Figs. 11 and 12), recorded ground motions within İzmir metropolitan area (indicated by black markers) are systematically underestimated by the median estimates of all tested GMMs. This could be due to significant site amplification at these periods, imposed by basin effects and ground response, which were thoroughly discussed in Gülerce et al. (2021) and Cetin et al. (2021).

6 Conclusions

In this study, we presented accelerometric data from the 30 October 2020 Samos earthquake recorded by Greek and Turkish National Strong Motion Networks at epicentral distances up to 200 km. We examined acceleration time histories, as well as Fourier amplitude spectra and 5% damped-response spectra, in accordance with the source-to-site distances and site classes of the recording stations. The entire dataset is available through online

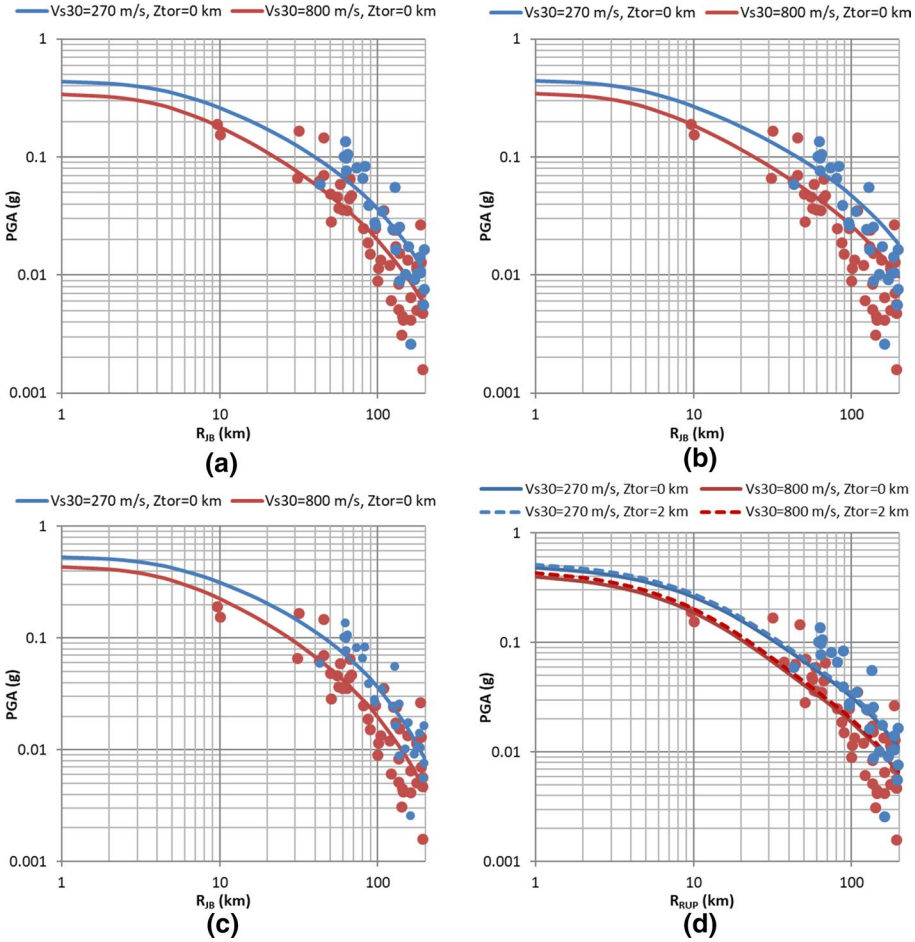

Fig. 7 Comparison of distance attenuation of PGA from global ground motion models with recorded values from the M7.0 Samos earthquake: **a** for BSSA14 model, global anelastic attenuation, **b** for BSSA14 model, anelastic attenuation for China and Turkey **c** for BSSA14 model, anelastic attenuation for Japan and Italy **d** for CY14 model. Blue and red curves are the median predictions for $V_{S30}=270$ m/s and $V_{S30}=800$ m/s, respectively, whereas blue and red symbols are associated with stations of $V_{S30}<360$ m/s and $V_{S30}\geq 360$ m/s, respectively. In d) two different values of parameter Ztor, the depth to the top of rupture, have been tested: Ztor = 0 km (continuous curves) and Ztor = 2 km (dashed curves)

sources and metadata, including station information, peak ground motion values, distance metrics and site classification as electronic supplementary material of this work.

The comparative examination of acceleration time histories and spectra around the M7.0 Samos earthquake source provide evidence for potential source effects at long periods (0.5–1.5 s), which requires further investigation of the rupture process (Kiratzi et al. 2021). This effect that appears as elevated energy within the afore-mentioned period range, has been observed at both soil and rock recording sites in İzmir metropolitan area. For the softer sites located within İzmir basin, a combination of source, basin and local site effects led to elevated long-period spectral acceleration content and overall longer significant

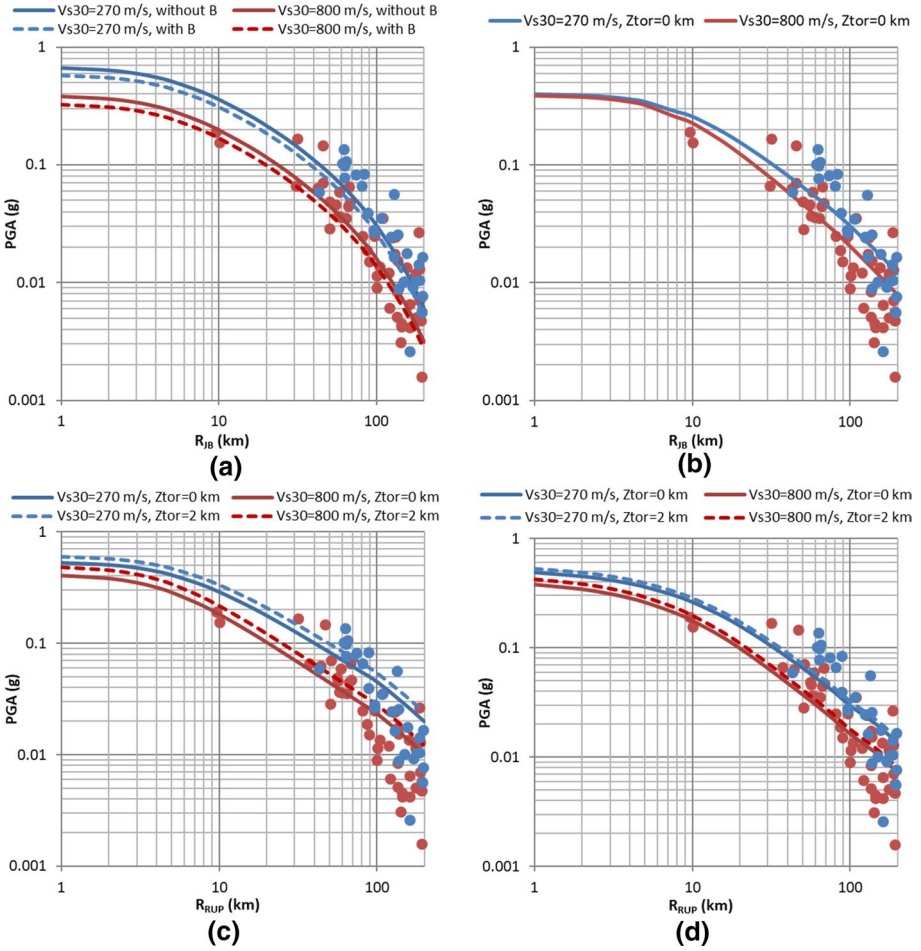

Fig. 8 Comparison of PGAs from the M7.0 Samos earthquake with distance attenuation of regional or regionally-adjusted ground motion prediction models: **a** Boore et al., (2021) model proposed for Greece, **b** KAAH15 model proposed for Turkey, **c** Turkey-adjusted AS08 model and **d** Turkey-adjusted CY08 model. Blue and red curves are the median estimates for $V_{S30}=270$ m/s and $V_{S30}=800$ m/s, respectively. Blue and red symbols belong to stations with $V_{S30}<360$ m/s and $V_{S30}>360$ m/s, respectively. Dashed and continuous curves correspond to different tested values of specific parameters of the GMMs, described on top of corresponding subplots

durations. These phenomena coupled with poor structural design yielded severe damages in multiple 7–9 story buildings near Bayraklı region. Comparisons in İzmir bay area indicate that despite the long-period amplification at some sites, the recorded response spectra are below the current and previous seismic design codes in Turkey. This implies that the building stock in Izmir contains weak structures, which failed due to ground motions arising from a source 70 km far away. Considering the seismic hazard in the region coupled with the basin structure, strengthening or reconstruction of the poor building stock should be performed before another large event occurs in the area.

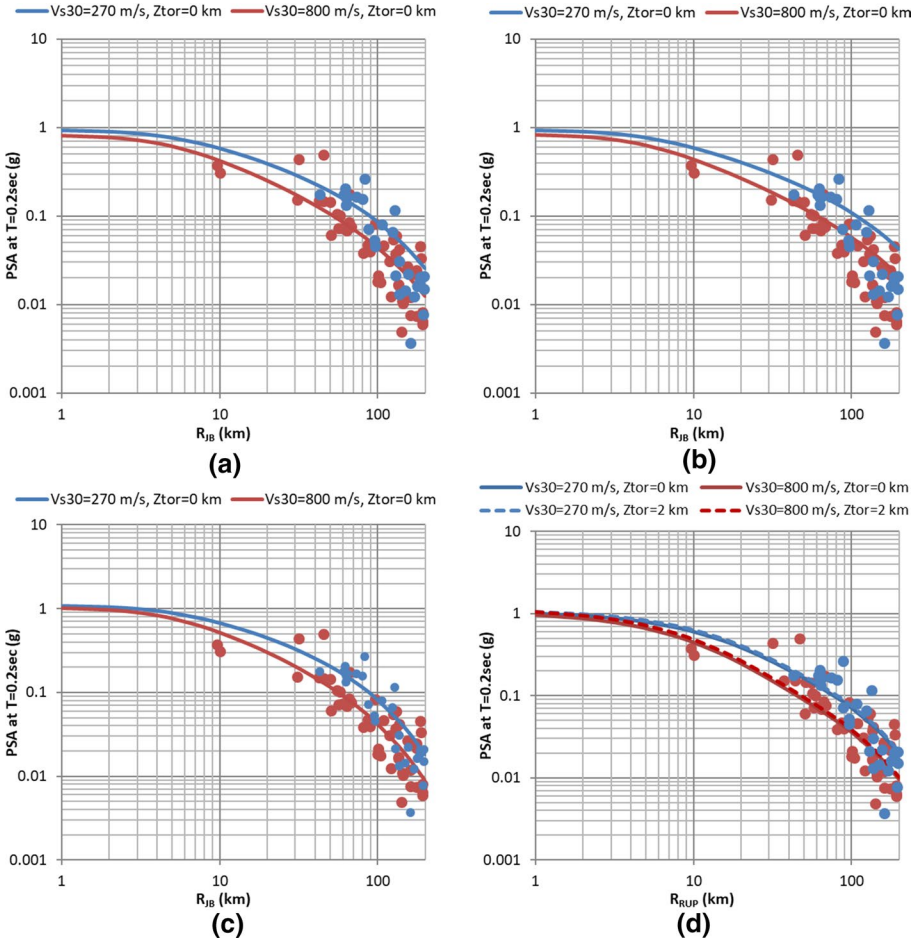

Fig. 9 Attenuation of spectral acceleration at T = 0.2 s of the M7.0 Samos earthquake data (dot symbols) and global ground motion prediction models: **a** for BSSA14 model, global anelastic attenuation, **b** for BSSA14 model, anelastic attenuation for China and Turkey **c** for BSSA14 model, anelastic attenuation for Japan and Italy **d** for CY14 model. Blue and red curves are the median estimates for $V_{S30} = 270$ m/s and $V_{S30} = 800$ m/s, respectively. Blue and red symbols correspond to stations with $V_{S30} < 360$ m/s and $V_{S30} > 360$ m/s, respectively. In d) two different values of parameter Ztor, the depth to the top of rupture, have been tested: Ztor = 0 km (continuous curves) and Ztor = 2 km (dashed curves)

Next, recorded peak ground motions in our merged dataset have been used in combination with region-specific empirical relations to produce an MMI-based macroseismic intensity map, based solely on instrumental observations. The resulting map with a maximum MMI value of VIII in areas of severe damage matches closely the spatial distribution of the observed damage pattern. These maps are mostly employed to coordinate rapid response in the aftermath of large events. It is thus, particularly important to have dense strong motion networks and regional correlations between instrumental and macroseismic intensity in seismically-active areas.

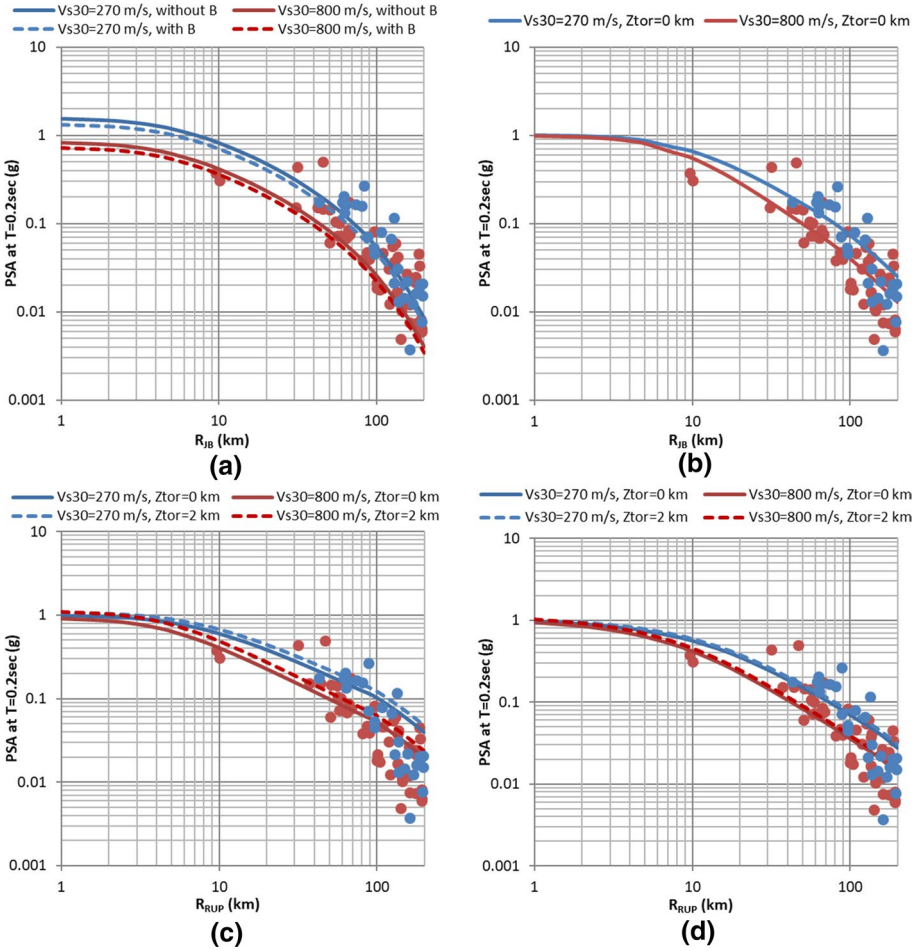

Fig. 10 Comparison of PSA values at T = 0.2 s from the M7.0 Samos earthquake with regional or regionally-adjusted ground motion prediction models: **a** Boore et al., (2021) model proposed for Greece, **b** KAAH15 model proposed for Turkey, **c** Turkey-adjusted AS08 model and **d** Turkey-adjusted CY08 model. Blue and red curves are the median estimates for V_{S30} = 270 m/s and V_{S30} = 800 m/s, respectively. Blue and red symbols belong to stations with V_{S30} < 360 m/s and V_{S30} > 360 m/s, respectively. Dashed and continuous curves correspond to different tested values of specific parameters of the GMMs, described on top of corresponding subplots

Comparisons of the M7.0 Samos earthquake data with several global, regional, and regionally-adjusted GMMs showed that the most recently proposed GMM by Boore et al. (2021) for the area of Greece best replicates the observed attenuation of peak ground motions (PGA and PSA at T = 0.2 s and T = 1.0 s) throughout the entire range of examined distance. This model captures the well-known fast attenuation of seismic waves and their amplitudes in the Aegean area and, thus, it is reasonable to expect that it would perform better for data from stations to the west of the Samos earthquake epicenter. However, prior knowledge and GMM testing on Turkish strong motion data have not provided similar indication for fast attenuation across the Turkish mainland. Thus, the deviations of median

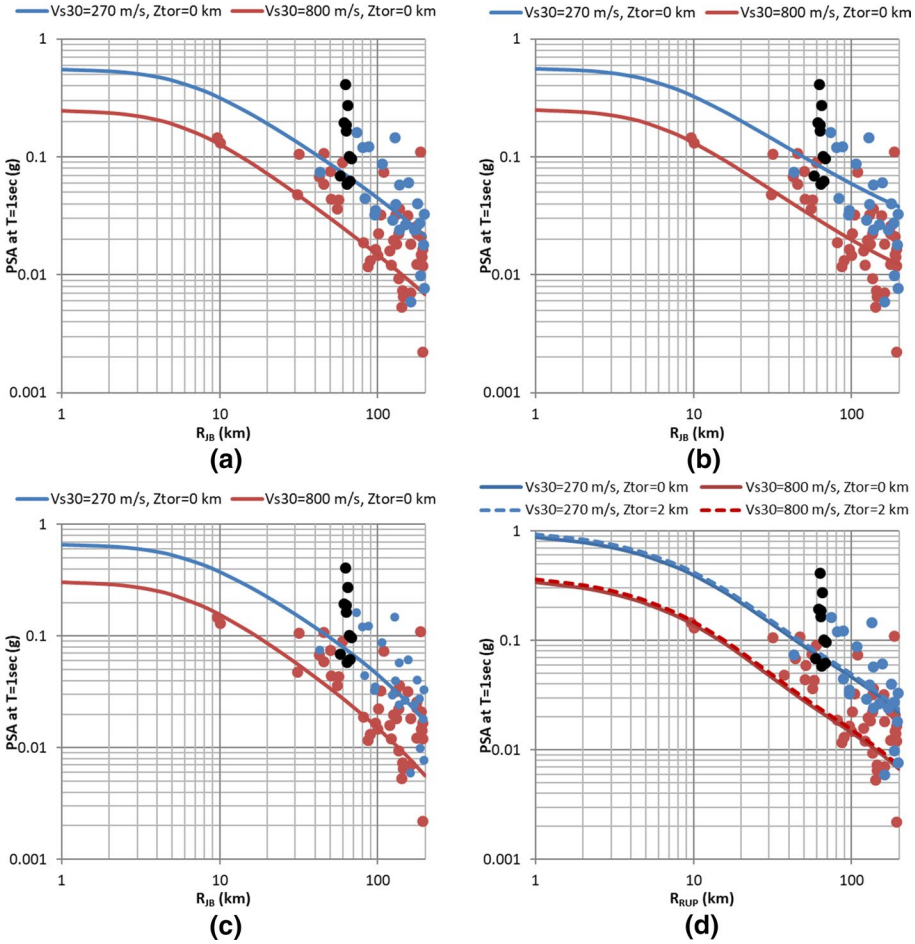

Fig. 11 Attenuation of spectral acceleration at T = 1.0 s of the M7.0 Samos earthquake data (dot symbols) and global ground motion prediction models: **a** for BSSA14 model, global anelastic attenuation, **b** for BSSA14 model, anelastic attenuation for China and Turkey **c** for BSSA14 model, anelastic attenuation for Japan and Italy **d** for CY14 model. Blue and red curves are the median estimates for $V_{S30} = 270$ m/s and $V_{S30} = 800$ m/s, respectively. Blue and red symbols correspond to stations with $V_{S30} < 360$ m/s and $V_{S30} > 360$ m/s, respectively. In d) two different values of parameter Ztor, the depth to the top of rupture, have been tested: Ztor = 0 km (continuous curves) and Ztor = 2 km (dashed curves). In all panels, black circles represent recorded ground motions within İzmir metropolitan area

predictions of regional and regionally-adjusted GMMs for Turkey from the M7.0 Samos observations require further investigation.

Future research should focus on comparisons of ground motion attenuation trends in Turkey and in Greece, not only close to large ruptures, but also to distances beyond 100 km. It is of interest, in this way, to verify whether the attenuation trend observed in this event, can be related to common regional characteristics appearing systematically or it is an event-specific observation. Similarly, studies on stress drop and geometrical spreading could also be performed within the context of regionally-adjustable ground motion models. As another future effort, in parallel to derivation of detailed source models of the Samos

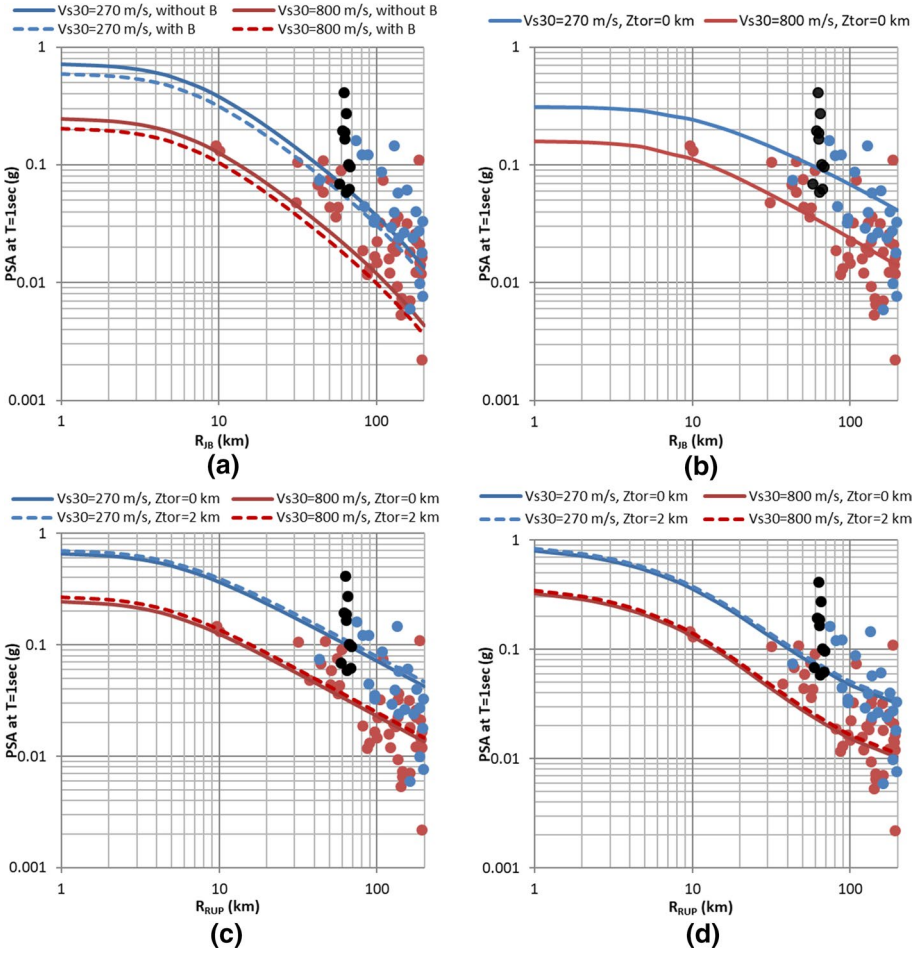

Fig. 12 Comparison of PSA values at T = 1.0 s from the M7.0 Samos earthquake with regional or regionally-adjusted ground motion prediction models: **a** Boore et al., (2021) model proposed for Greece, **b** KAAH15 model proposed for Turkey, **c** Turkey-adjusted AS08 model and **d** Turkey-adjusted CY08 model. Blue and red curves are the median estimates for V_{S30} = 270 m/s and V_{S30} = 800 m/s, respectively. Blue and red symbols belong to stations with V_{S30} < 360 m/s and V_{S30} > 360 m/s, respectively. Dashed and continuous curves correspond to different tested values of specific parameters of the GMMs, described on top of corresponding subplots. In all panels, black circles represent recorded ground motions within İzmir metropolitan area

earthquake, ground motion simulations of this event and potential scenario earthquakes in the region would augment existing data and conclusions.

Supplementary Information The online version contains supplementary material available at https://doi.org/10.1007/s10518-021-01251-5.

Acknowledgements The reconnaissance studies of METU faculty were supported by Middle East Technical University. We acknowledge this support. We also acknowledge the support from the Hellenic Association of Earthquake Engineering, Earthquake Engineering Association of Turkey, Earthquake Foundation of Turkey, Earthquake Engineering Research Institute (USA) and Geotechnical Extreme Events Reconnaissance

Association. Maps of Figures 1 and 3 were created using the Generic Mapping Tools software (http://gmt.soest.hawaii.edu/). We thank Sinan Akkar and Aybige Akıncı for their careful and constructive reviews of the manuscript.

Funding Parts of this research have been funded by Middle East Technical University, Hellenic Association of Earthquake Engineering, Earthquake Engineering Association of Turkey, Earthquake Foundation of Turkey and Earthquake Engineering Research Institute (USA) and Geotechnical Extreme Events Reconnaissance Association.

Availability of data and material All data and metadata pertinent to this work are available either through the supplementary online resources or through web portals with references in the text.

Code availability No code was developed in the frame of this study.

Conflict of interest The authors have no financial or proprietary interests in any material discussed in this article.

References

Abrahamson NA, Silva WJ (2008) Summary of the Abrahamson and Silva NGA ground motion relations. Earthq Spectra 24(1):67–97. https://doi.org/10.1193/1.2924360

Abrahamson NA, Silva WJ, Kamai R (2014) Summary of the ASK14 ground-motion relation for active crustal regions. Earthq Spectra 30(3):1025–1057. https://doi.org/10.1193/070913EQS198M

Akinci A, Cheloni D, Dindar AA (2021) The 30 October 2020, M7. 0 Samos Island (Eastern Aegean Sea) Earthquake: effects of source rupture, path and local-site conditions on the observed and simulated ground motions. Bulletin of Earthquake Engineering, 1–27

Akkar S, Aldemir A, Askan A, Bakır S, Canbay E, Demirel İO, Erberik MA, Gülerce Z, Gülkan P, Kalkan E, Prakash S, Sandikkaya MA, Sevilgen V, Ugurhan B, Yenier E (2011) 8 March 2010 Elazıg-Kovancılar (Turkey) earthquake: Observations on ground motions and building damage. Seismol Res Lett 82(1):42–58. https://doi.org/10.1785/gssrl.82.1.42

Akkar S, Çağlar NM, Kale Ö, Yazgan U, Sandıkkaya MA (2021) Impact of rupture-plane uncertainty on earthquake hazard: observations from the 30 October 2020 Samos earthquake. Bull Earthq Eng 19(7):2739–2761

Allen TI, Wald DJ (2009) On the use of high-resolution topographic data as a proxy for seismic site conditions (VS30). Bull Seism Soc Am 99(2):935–943. https://doi.org/10.1785/0120080255

Ansal A, Abrahamson N, Bardet JP, Barka A, Baturay MB, Berilgen BM, Boulanger R, Bray J, Cetin O, Cluff L, Durgunoglu T, Erten D, Erdik M, Frost D, Idriss IM, Karadayilar T, Kaya A, Lettis W, Martin J, Mitchell J, Olgun G, O'Rouke T, Paige W, Rathje E, Roblee C, Sancio R, Savage W, Seed R, Somerville P, Stewart J, Sunman B, Swan B, Toprak S, Ural D, Yashinski M, Yilmaz T, Youd L (1999a) Initial geotechnical observations of the August 17, 1999 Kocaeli earthquake: a report of the Turkey-US geotechnical earthquake engineering reconnaissance team. Geotechnical Extreme Event Reconnaissance Association (GEER) Report 001. https://doi.org/10.18118/G6CC7F

Ansal A, Bardet JP, Barka A, Baturay MB, Berilgen M, Bray J, Cetin O, Cluff L, Durgunoglu T, Erten D, Erdik M, Idriss IM, Karadayilar T, Kaya A, Lettis W, Olgun G, Paige W, Rathje E, Roblee C, Stewart J, Ural D (1999b) Initial geotechnical observations of the November 12, 1999, Duzce earthquake. Geotechnical Extreme Event Reconnaissance Association (GEER) Report 003. https://doi.org/10.18118/G63W27

Bilal M, Askan A (2014) Relationships between Felt Intensity and Recorded Ground-Motion Parameters for Turkey. Bull Seism Soc Am 104(1):484–496. https://doi.org/10.1785/0120130093

Boore DM (2010) Orientation-independent, non geometric-mean measures of seismic intensity from two horizontal components of motion. Bull Seism Soc Am 100:1830–1835. https://doi.org/10.1785/0120090400

Boore DM, Stewart JP, Seyhan E, Atkinson GA (2014) NGA-West 2 equations for predicting PGA, PGV, and 5%-damped PSA for shallow crustal earthquakes. Earthq Spectra 30(3):1057–1087. https://doi.org/10.1193/070113EQS184M

Boore D, Stewart JP, Skarlatoudis A, Seyhan E, Margaris B, Theodoulidis N, Scordilis E, Kalogeras I, Klimis N, Melis N (2021) A Ground-motion prediction model for shallow crustal earthquakes in Greece. Bull Seism Soc Am 111(2):857–874. https://doi.org/10.1785/0120200270

Campbell KW, Bozorgnia Y (2008) NGA ground motion model for the geometric mean horizontal component of PGA, PGV, PGD and 5% damped linear elastic response spectra for periods ranging from 0.01 to 10 s. Earthq Spectra 24(1):139–173. https://doi.org/10.1193/1.2857546

Campbell KW, Bozorgnia Y (2014) NGA-West2 ground motion model for the average horizontal components of PGA, PGV, and 5%-damped linear acceleration response spectra. Earthq Spectra 30(3):1087–1117. https://doi.org/10.1193/062913EQS175M

CBCEA, Code for Buildings Constructed in Earthquake Areas (2007), Ministry of Public Works and Settlement Ankara, Turkey

Cetin OK (2020) Preliminary report on engineering and geological effects of the January 24, 2020 magnitude 6.7 earthquake in Elazig, Turkey. Geotechnical Extreme Event Reconnaissance Association (GEER) Report 065. https://doi.org/10.17603/ds2-9jz1-e287

Cetin OK, Mylonakis G, Sextos A Stewart JP (2020) Seismological and engineering effects of the M7.0 Samos Island (Aegean Sea) earthquake. Geotechnical Extreme Event Reconnaissance Association (GEER) Report 069. https://doi.org/10.18118/G6H088

Cetin OK, Altun S, Askan A, Akgün M, Sezer A, Kıncal C et al. (2021) The Site Effects of October 30 2020, M7.0 Samos Island (Aegean Sea) Earthquake in Izmir Bay. Soil Dyn. Earthq. Eng., submitted

Chiou BSJ, Youngs RR (2008) Chiou-Youngs NGA ground motion relations for the geometric mean horizontal component of peak and spectral ground motion parameters. Earthq SpectRa 24(1):173–217. https://doi.org/10.1193/1.2894832

Chiou BSJ, Youngs RR (2014) Update of the Chiou and Youngs NGA model for the average horizontal component of peak ground motion and response spectra. Earthq Spectra 30(3):1117–1155. https://doi.org/10.1193/072813EQS219M

CSCDA, Code for Structures Constructed in Disaster Areas (1975), Ministry of Public Works and Settlement Ankara, Turkey

Earthquake Protection and Planning Organization – EPPO/OASP (2000) Greek Seismic Code (EAK2000), Athens, Greec

EC8 (2004) Eurocode 8: Design of structures for earthquake resistance. Part 1: General rules, seismic actions and rules for buildings, European Norm, Management centere: Rue de Stassart 36, B-1050 Brussels, Belgium

Erberik MA (2008) Fragility-based assessment of typical mid-rise and low-rise RC buildings in Turkey. Eng Struct 30(5):1360–1374

Gülerce Z, Kargıoğlu B, Abrahamson NA (2016) Turkey-adjusted NGA-W1 horizontal ground motion prediction models. Earthq Spectra 32(1):75–100. https://doi.org/10.1193/022714EQS034M

Gülerce Z, Akbaş B, Özacar AA, Sopacı E, Önder FM, Uzel B, et al. (2021) Predictive Performance of Current Ground Motion Models for Recorded Strong Motions in 2020 Samos Earthquake. Soil Dyn. Earthq. Eng., submitted.

Joyner WB, Boore DM (1981) Peak horizontal acceleration and velocity from strong-motion records including records from the 1979 Imperial Valley, California, earthquake. Bull Seism Soc Am 71(6):2011–2038

Kale Ö (2019) Some Discussions on Data-Driven Testing of Ground-Motion Prediction Equations under the Turkish Ground-Motion Database. J Earthquake Eng 23(1):160–181. https://doi.org/10.1080/13632469.2017.1323047

Kale O, Akkar S, Ansari A, Hamzehloo H (2015) A ground-motion predictive model for Iran and Turkey for horizontal PGA, PGV, and 5% damped response spectrum: Investigation of possible regional effects. Bull Seism Soc Am 105(2A):963–980. https://doi.org/10.1785/0120140134

Kiratzi A, Papazachos C, Özacar A, Pinar A, Kkallas Ch, Sopaci E (2021) Characteristics of the 2020 Samos earthquake (Aegean Sea) using seismic data. Bull Earthq Eng, submitted

Margaris B, Papaioannou Ch, Theodoulidis N, Savvaidis A, Klimis N, Makra K, Karakostas Ch, Lekidis V, Makarios T, Salonikios T, Demosthenus M, Athanasopoulos G, Mylonakis G, Papantonopoulos G, Efthymiadou V, Kloukinas P, Ordonez I, Vlachakis V, Stewart JP (2008) Preliminary report on the principal seismological and engineering aspects of the M_w=6.5 Achaia-Ilia (Greece) earthquake on 8 June 2008. Geotechnical Extreme Event Reconnaissance Association (GEER) Report 013. https://www.doi.org/https://doi.org/10.18118/G6TG64

Margaris B, Scordilis E, Stewart JP, Boore DM, Theodoulidis N, Kalogeras I, Melis N, Skarlatoudis A, Klimis N, Seyhan E (2021) Hellenic strong-motion database with uniformly assigned source and site metadata for the time-period 1972–2015. Seism Res Lett. https://doi.org/10.1785/0220190337

Nikolaou S, Zekkos D, Assimaki D, Gilsanz R (2014) GEER/EERI/ATC earthquake reconnaissance January 26th/February 2nd 2014 Cephalonia, Greece Events. Geotechnical Extreme Event Reconnaissance Association (GEER) Report 034. https://www.doi.org/https://doi.org/10.18118/G63S3K

Paolucci R, Pacor F, Puglia R, Ameri G, Cauzzi C, Massa M (2011) Record Processing in ITACA, the New Italian Strong-Motion Database. In: Akkar S, Gülkan P, van Eck T (eds) Earthquake Data in Engineering Seismology. Geotechnical, Geological, and Earthquake Engineering, vol 14. Springer, Dordrecht. http://doi-org-443.webvpn.fjmu.edu.cn/https://doi.org/10.1007/978-94-007-0152-6_8

Power M, Chiou B, Abrahamson N, Bozorgnia Y, Shantz T, Roblee C (2008) An overview of the NGA project. Earthq Spectra 24(1):3–21

Stewart JP, Klimis N, Savvaidis A, Theodoulidis N, Zargli E, Athanasopoulos G, Pelekis P, Mylonakis G, Margaris B (2014) Compilation of the local Vs profile database and its application for inference of V_{s30} from geologic- and terrain-based proxies. Bull Seis Soc Am 104(6):2827–2841. https://doi.org/10.1785/0120130331

TBEC, Turkish Building Earthquake Code (2019) Ministry of Interior, Disaster and Emergency Management Presidency (AFAD), Ankara, Turkey

Authors and Affiliations

Aysegul Askan[1] · Zeynep Gülerce[1] · Zafeiria Roumelioti[2] · Dimitris Sotiriadis[3] · Nikolaos S. Melis[4] · Abdullah Altindal[1] · Burak Akbaş[1] · Eyüp Sopaci[5] · Shaghayegh Karimzadeh[1,9] · Ioannis Kalogeras[4] · Nikolaos Theodoulidis[6] · Kiriaki Konstantinidou[6] · A. Arda Özacar[7] · Özkan Kale[8] · Basil Margaris[6]

[1] Department of Civil Engineering, Middle East Technical University, Ankara, Turkey

[2] Department of Geology, University of Patras, Patras, Greece

[3] Department of Civil Engineering, Democritus University of Thrace, Xanthi, Greece

[4] Institute of Geodynamics, National Observatory of Athens, Athens, Greece

[5] Deparment of Geodetic and Geographical Information Technologies, Middle East Technical University, Ankara, Turkey

[6] Institute of Engineering Seismology and Earthquake Engineering, Thessaloniki, Greece

[7] Deparment of Geological Engineering, Middle East Technical University, Ankara, Turkey

[8] Deparment of Civil Engineering, Ted University, Ankara, Turkey

[9] Institute for Sustainability and Innovation in Structural Engineering (ISISE), Now at University of Minho, Braga, Portugal